A multi-grid extended finite element method for elastic crack growth simulation

Johann Rannou, Anthony Gravouil, Alain Combescure

A multi-grid extended finite element method for elastic crack growth simulation

Johann Rannou — Anthony Gravouil — Alain Combescure

LaMCoS, INSA-Lyon, CNRS UMR5259
18 - 20, rue des Sciences F-69621 Villeurbanne
johann.rannou@insa-lyon.fr

ABSTRACT. *The eXtended Finite Element Method (*X-FEM*) has been applied to a wide range of applications, in particular for crack growth simulations in structural mechanics. However, for real applications (engineering simulations,...), even if one does not need to mesh the crack, it is necessary to take into account the different spatial scales linked to the size of the domain, the geometry of the boundary, the size of the boundary with prescribed displacement or loading, the discretized "representation" of the crack,... In this respect, one proposes in this paper to couple the eXtended Finite Element Method with a multi-grid strategy. Details are given for numerical implementation with a hierarchical finite element strategy. Finally, some examples are given (mixed mode crack growth simulations) to validate the method.*

RÉSUMÉ. *La méthode des éléments finis étendus (*X-FEM*) a été appliquée à de nombreux domaines de mécanique des structures, en particulier à la simulation de propagation de fissures. Cependant, pour des applications industrielles, même si la fissure ne nécessite pas d'être maillée explicitement, les différentes échelles spatiales associées à la géométrie de la structure, à celle de la fissure, aux conditions aux limites, etc., doivent être prises en compte. Pour cela, nous proposons dans cet article de coupler la méthode des éléments finis étendus à la stratégie multigrille. L'implémentation numérique dans le cadre d'éléments finis hiérarchiques est précisée. Des exemples de propagation de fissure en mode mixte sont ensuite donnés pour valider la méthode.*

KEYWORDS: *extended finite element method, multi-grid solver, crack growth simulations.*

MOTS-CLÉS : *éléments finis étendus, multigrille, propagation de fissure.*

1. Introduction

Literature on the coupling between the finite element method and different multi-scale strategies is rapidly expanding, on the one hand due to the improvement of multi-grid solvers (Lubrecht *et al.,* 2000, Brandt, 1977, Parsons *et al.,* 1990a, Gravouil *et al.,* 2003), or on the other hand due to the increasing of knowledge on the nonlinear behaviour of the microstructure (Fish *et al.,* 2004, Stazi, 2003, Feyel, 2003). In this presentation, our goal is to focus on improving the numerical treatment of engineering applications in presence of discontinuities. In this respect, the eXtended Finite Element Method is well suited to describe a discontinuity incompatible with the discretization of the structure (Moës *et al.,* 1999). In this case, one can consider the mesh of the structure as a "coarse spatial scale" and the discontinuity as a "fine spatial scale" (Guidault *et al.,* 2005). As a consequence, even in the case of X-FEM, one has to define the mesh of the structure sufficiently fine to be able to "describe" the geometry of the discontinuity (cf. Figure 1). Furthermore, other fine spatial scales can be considered to improve the initial fixed mesh: complex geometry of the boundary, the description of time evolving prescribed displacement or loading, or zone with high stress gradients (Ribeaucourt *et al.,* 2005, Elguedj *et al.,* 2005). For that purpose, one proposes to couple the X-FEM with a multi-grid strategy which allows to "capture" all the spatial scales of the problem. In all this paper, one makes the assumption that the linear fracture mechanics is valid for every scales. Furthermore, one considers that a topological enrichment strategy (Béchet *et al.,* 2005) is sufficient to describe the K-dominated area.

In the first part, one describes the multi-grid strategy in a general point of view. In the second part, one discusses the development of multi-scale operators in the context of X-FEM, then one proposes a specific implementation in the case of crack discontinuity. In the last part, validation studies are proposed for mixed mode crack growth simulation.

2. Multi-grid strategy

The principle of multi-grid methods is based on the fact that iterative solvers are efficient to capture the high frequency part of the solution, and less efficient to calculate the low frequency part of the solution (Brandt, 1977, Parsons *et al.,* 1990a, Parsons *et al.,* 1990b). In this respect, a point of departure is to consider different grids (meshes) which are able to capture efficiently the different spatial scales of the solution.

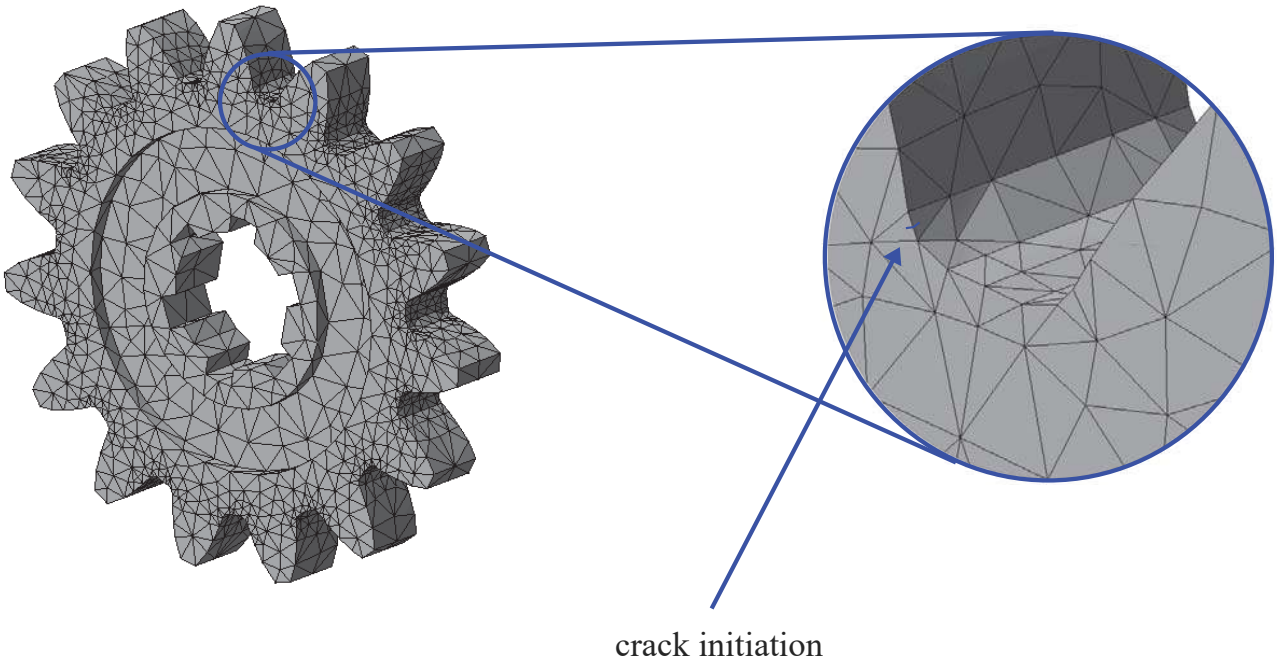

Figure 1. *Example of an engineering mesh where a multi-scale approach is needed*

2.1. *The two grids algorithm*

One considers a linear problem discretized on a fine mesh m and a coarse mesh M. The problem can be written as follow:

$$K_m U_m = F_m \qquad \text{on the fine mesh} \qquad [1]$$

$$K_M U_M = F_M \qquad \text{on the coarse mesh} \qquad [2]$$

where respectively U, K and F are the discretized displacement, stiffness matrix and external loading for each spatial scale.

The multi-grid algorithm for a linear problem can be described with the 6 following steps for the k^{th} iteration.

Beginning of cycle k

– First relaxation step

One initializes the k^{th} cycle with the previous approximation U_m^{k-1} and one proceeds to ν_1 iterations (in practice of the order of 2 to 5). One obtains the new approximation $\widetilde{U}_m^k$. The number ν_1 is fixed in the aim to decrease sufficiently the high frequency error defined by:

$$E_m = U_m - \widetilde{U}_m^k \qquad [3]$$

The idea is then to try to reduce the low frequency error only on the coarse mesh. For that purpose, one define the residual as follow:

$$R_m = F_m - K_m \widetilde{U}_m^k \qquad [4]$$

Moreover, K_m is a linear operator, one then has:

$$K_m E_m = R_m \quad [5]$$

– Restriction step

The residual is now smooth and it can be well represented on the coarse mesh. One defines I_m^M as the restriction operator from the fine scale to the coarse scale. In this respect, one transfers the residual from the fine mesh to the coarse mesh:

$$R_M = I_m^M R_m \quad [6]$$

– Resolution of the coarse problem

$$K_M \Delta U_M = R_M \quad [7]$$

where ΔU_M is the low frequency correction term. Because E_m is smooth, ΔU_M should be a good approximation of it.

– Prolongation step

One defines I_M^m as the prolongation operator from the coarse scale to the fine scale. In this respect, one transfers the coarse correction term on the fine scale:

$$\Delta U_m = I_M^m \Delta U_M \quad [8]$$

– Correction step

ΔU_m is assumed to be a good approximation of E_m. Then, according to [3] :

$$\widetilde{\widetilde{U}}_m^k = \widetilde{U}_m^k + \Delta U_m \quad [9]$$

where $\widetilde{\widetilde{U}}_m^k$ is the updated solution. The first term on the right hand side represents the high frequency contribution $\widetilde{U}_m^k$ to the solution and the second one the low frequency contribution.

– Second relaxation step

If needed, a second relaxation step (in practice of the order of 1 to 3 iterations) is introduced in order to eliminate any high frequency error resulting from the prolongation step. The new approximation of U_m at the end of cycle k is now U_m^k.

End of cycle k

One obtains the convergence of the algorithm when the following criterion is true:

$$||R_m|| < \varepsilon \quad [10]$$

Furthermore, it can be noticed that the resolution of the coarse problem can be done either with a direct solver or recursively with a limited number of multi-grid cycles

γ with a third coarser mesh, and so on (Lubrecht *et al.,* 2000). Thus, the parameters of multi-grid methods consist of not only the number of grids involved, but also the manner in which the transition between scales is achieved. It can be schown that such approaches can converge in $O(n)$, n is a parameter linked to the size of the discretized problem (Parsons *et al.,* 1990a), which can be compared to other iterative solvers like Gauss-Seidel ($O(n^2)$) or conjugate gradient solvers ($O(n^{3/2})$).

2.2. *Multi-scale operators*

One has previously used restriction and prolongation operators I_m^M and I_M^m. In practice, these operators transfer nodal fields from the fine mesh to the coarse one and inversely (Dureisseix, n.d.). One can also build these two operators by preserving the internal work on the different scales. As a consequence, it can be shown that one obtain the following relation:

$$I_m^M = {I_M^m}^T \quad [11]$$

Furthermore, it justifies the dual property of the two operators, where the first one is used to reduce the residual forces, and the second one to prolong the displacement increment.

A classical way to build the prolongation operator is to use the shape functions to interpolate the displacement field of the coarse scale to the fine scale. Then, the values of the shape functions of the coarse mesh is related to the nodes of the fine mesh in a rectangular matrix.

3. Multi-scale operators and enrichment

3.1. *Extended finite element method*

The extended finite element method proposes to enrich locally the finite element discretization (which is a particular case of the so called partition of unity method) (Melenck *et al.,* 1996, Moës *et al.,* 1999). These enrichments have to capture the displacement discontinuity and its asymptotic behaviour close to the crack tip independently of the mesh. For instance, if one considers a fixed spatial scale represented by a finite element mesh, the displacement field $\underline{u}(\underline{x})$ is:

$$\underline{u}(\underline{x}) = \sum_{i \in \mathcal{N}}^{n} N_i(\underline{x})\underline{u}_i + H(\underline{x}) \sum_{i \in \mathcal{N}_{cut}} N_i(\underline{x})\underline{a}_i + \sum_{j=1}^{4} \gamma_j(\underline{x}) \left(\sum_{i \in \mathcal{N}_{sing}} N_i(\underline{x})\underline{b}_{ji} \right) \quad [12]$$

where $\mathcal{N}$ is the set of nodes of the mesh, $N_i(\underline{x})$ the shape function associated with node i. $\underline{u}_i$ are the classical degrees of freedom, and a_i, b_{1i}, b_{2i}, b_{3i}, b_{4i} the additional degrees of freedom linked to the additional functions of enrichment H,γ_1,γ_2,γ_3,γ_4. It can be noticed that these additional functions are defined independently of any

discretization: their local contribution is only represented by their product with the classical shape functions $N_i(\underline{x})$ (cf. Figure 4a for γ_1). In this paper, one chooses a topological enrichment by the fact that $\mathcal{N}_{cut}$ only contains the nodes of the elements completely cut by the crack, and $\mathcal{N}_{sing}$ the nodes of the elements containing the crack tip. On Figure 2 one illustrates the strategy of local enrichment for a coarse and a fine mesh. The topological enrichment is here prefered to the geometrical one (Béchet *et al.,* 2005) because one makes the assumption that at each discretization level, the singular enriched area is sufficient to well describe the K-dominated area. However, all the issues encoutered with a geometrical enrichment strategy should be the same that the one dicussed below and the strategy adopted should be fitable to geometrical enrichment.

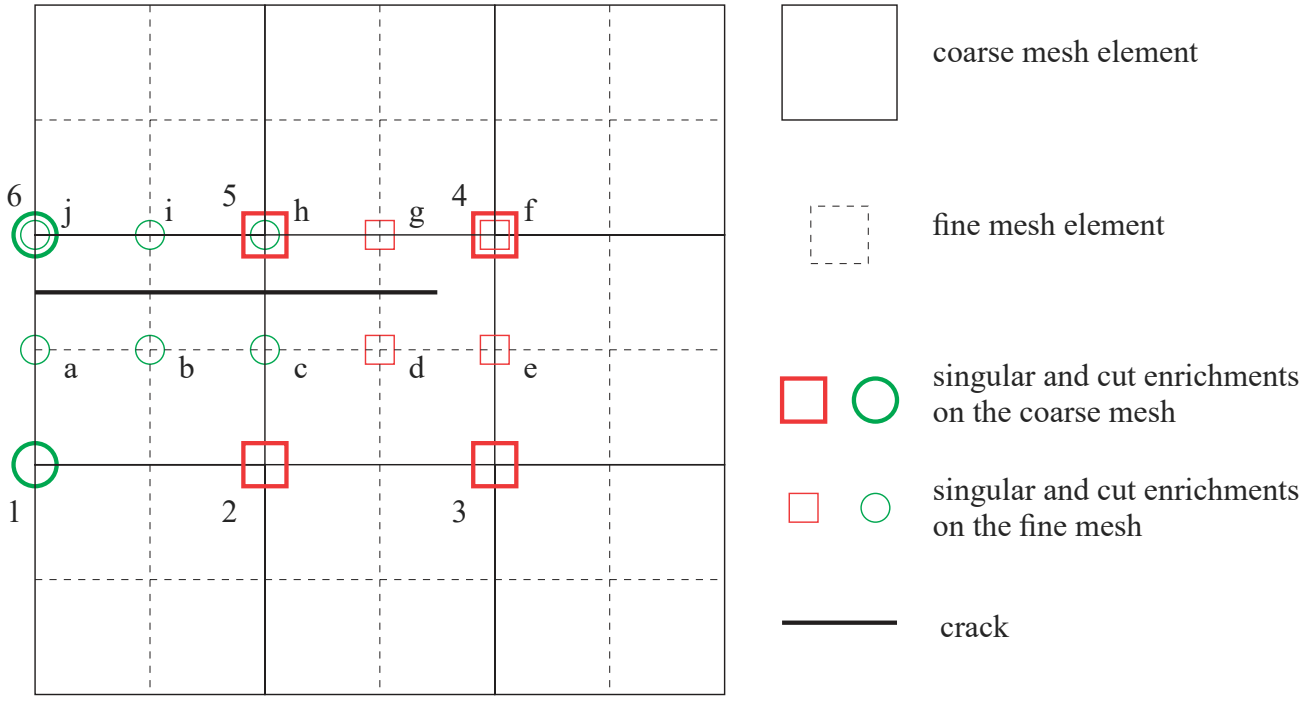

Figure 2. *Overprinted coarse and fine meshes. Number and letters are respectively related to the nodes of the coarse and the fine mesh*

3.2. *Formulation of the interpolation problem between two grids and their enrichments*

We remind that in this paper, all grids are enriched with a topological X-FEM strategy. The two multi-scale operators are linked by the relation [11], this is why one only focuses on the definition of the prolongation operator. Its role is to define kinematics quantities $\underline{u}^f$ on the fine mesh $\mathcal{M}_f$ from kinematics quantities $\underline{u}^c$ on the coarse mesh $\mathcal{M}_c$. Let us consider a non enriched node n of the fine mesh with the coordinates $\underline{x}_n$. Its degrees of freedom $\underline{u}^f_n$ are directly determined by the relation:

$$\underline{u}^f_n = \underline{u}^c(\underline{x}_n) \qquad [13]$$

If the node n is an enriched node, one can write in a general point of view:

$$\underline{u}_n^f + \underline{a}_n^f H(\underline{x}_n) + \sum_{j=1}^{4} \underline{b}_{jn}^f \gamma_j(\underline{x}_n) = \underline{u}^c(\underline{x}_n) \quad [14]$$

Degrees of freedom $\underline{u}_n^f$, $\underline{a}_n^f$, and $\underline{b}_{jn}^f$ are not defined here in a one-to-one way by $\underline{u}^c(\underline{x}_n)$. One can then distinguish the two following cases:

– degrees of freedom on the fine mesh can be one-to-one determined from the degrees of freedom of the coarse mesh. In such a case, one says that the enrichments of the node are compatible with the enrichments of the coarse mesh,

– degrees of freedom on the fine mesh can not be one-to-one determined from the degrees of freedom of the coarse mesh. In this case, one says that the enrichments of the node are incompatible with the enrichments on the coarse mesh.

Let us define $\mathcal{F} = \{f_i(\underline{x})\}$, the set of enrichment functions. Recall that these functions are independent on the discretization (cf. Figure 4a). Let us consider a node n of $\mathcal{M}_f$ with coordinates $\underline{x}_n$ enriched with a subset $\mathcal{F}_f \subset \mathcal{F}$. The displacement of this node can be written as:

$$\underline{u}^f(\underline{x}_n) = \underline{u}_n^f + \sum_{j \in \mathcal{F}_f} \underline{u}_{jn}^f f_j(\underline{x}_n) \qquad \forall \mathcal{F} \quad [15]$$

where $\underline{u}_n^f$ is the vector of standard degrees of freedom linked to the node n and $\underline{u}_{jn}^f$ is the vector of additional degrees of freedom linked to enrichment functions $f_j(\underline{x})$.

The displacement on the same coordinates $\underline{x}_n$ of the coarse mesh can also be written as:

$$\underline{u}^c(\underline{x}_n) = \sum_{i \in \mathcal{N}} N_i^c(\underline{x}_n) \left(\underline{u}_i^c + \sum_{j \in \mathcal{F}_f} \underline{u}_{ji}^c f_j(\underline{x}_n) + \sum_{j \in \mathcal{F} \setminus \mathcal{F}_f} \underline{u}_{ji}^c f_j(\underline{x}_n) \right) \quad \forall \mathcal{F} \quad [16]$$

where N_i^c are the shape functions linked to the coarse mesh. It can be shown that the enrichment is "compatible" if one verifies the following property:

$$\sum_{i \in \mathcal{N}} N_i^c(\underline{x}_n) \left(\sum_{j \in \mathcal{F} \setminus \mathcal{F}_f} \underline{u}_{ji}^c f_j(\underline{x}_n) \right) = 0 \quad [17]$$

Indeed, one can then write:

$$\begin{aligned} \underline{u}^f(\underline{x}_n) &= \underline{u}^c(\underline{x}_n) \\ \underline{u}_n^f + \sum_{j \in \mathcal{F}_f} \underline{u}_{jn}^f f_j(\underline{x}_n) &= \sum_{i \in \mathcal{N}} N_i^c(\underline{x}_n) \left(\underline{u}_i^c + \sum_{j \in \mathcal{F}_f} \underline{u}_{ji}^c f_j(\underline{x}_n) \right) \quad \forall \mathcal{F} \quad [18] \end{aligned}$$

As a consequence, it is possible to identify the degrees of freedom of $\mathcal{M}_f$ in a one-to-one way:

$$\left\{ \begin{array}{rcll} \underline{u}_n^f & = & \displaystyle\sum_{i \in \mathcal{N}} N_i^c(\underline{x}_n) \underline{u}_i^c & \\ & & & \\ \underline{u}_{jn}^f & = & \displaystyle\sum_{i \in \mathcal{N}} N_i^c(\underline{x}_n) \underline{u}_{ji}^c & \forall j \end{array} \right. \quad [19]$$

On the opposite case, (relation [17] is not verified), no identification is possible. Enrichment of node n is not compatible with the coarse mesh.

3.3. *Example of compatible and incompatible enrichments with X-FEM*

In this section, one considers the configuration defined in Figure 2. Furthermore, one defines the two sets of nodes on $\mathcal{M}_f$:

$$\mathcal{S}_1 = \{a, j, d, e, f, g\} \quad [20]$$

$$\mathcal{S}_2 = \{b, c, h, i\} \quad [21]$$

In this particular case, the first set of nodes $\mathcal{S}_1$ corresponds to compatible enrichments and the second one $\mathcal{S}_2$ to incompatible enrichments.

Indeed, for the first set of nodes $\mathcal{S}_1$, if one considers the nodes a and j of the fine mesh, one can write:

$$\mathcal{F}_f = \{H\} \quad [22]$$

$$\mathcal{F} \setminus \mathcal{F}_f = \{\gamma_1, \gamma_2, \gamma_3, \gamma_4\} \quad [23]$$

As can be seen on Figure 4b (where $\gamma_1(\underline{x}) \sum_{i \in \mathcal{N}_{sing}} (N_i(\underline{x}) b_{1i}) = 0$ in $\underline{x}_a$ and $\underline{x}_j$) the local nature of the singular enrichment involves that condition [17] is exactly verified for points of coordinate $\underline{x}_a$ and $\underline{x}_j$. For instance, one can write for the node a :

$$\underline{u}_a + \underline{a}_a H(\underline{x}) = 1/2\,(\underline{u}_1 + \underline{u}_6) + 1/2\,(\underline{a}_1 + \underline{a}_6)\,H(\underline{x}) \quad [24]$$

this expression is similar to [18] since the enrichment function is the same on the left hand side and the right hand side of the equality. As a consequence, one can proceed in a unique way to the following identification (cf. Equation [19]).

$$\underline{u}_a = 1/2\,(\underline{u}_1 + \underline{u}_6) \quad [25]$$

$$\underline{a}_a = 1/2\,(\underline{a}_1 + \underline{a}_6) \quad [26]$$

Concerning the nodes d, e, f and g the same analysis can be done with:

$$\mathcal{F}_f = \{\gamma_1, \gamma_2, \gamma_3, \gamma_4\} \quad [27]$$

$$\mathcal{F} \setminus \mathcal{F}_f = \{H\} \quad [28]$$

One can notice that this identification is similar to a prolongation step of the displacement field separately on each set of enrichment function. In the aim to illustrate this point, one can consider the one dimensional case of Figure 3. Only the enrichment function H is considered here. Enriched nodes are automatically compatible ones since:

$$\mathcal{F}_f = \{H\} = \mathcal{F} \quad \Longrightarrow \quad \mathcal{F} \setminus \mathcal{F}_f = \emptyset \qquad [29]$$

The displacement field can the be decomposed with a standard part and an enriched part as follows:

$$\underline{u}(x) = \underline{u}_{std}(x) + \underline{u}_H(x) \qquad [30]$$

Consequently, interpolate separately these two components of the displacement field on a finer mesh allows to prolong the total displacement field on it.

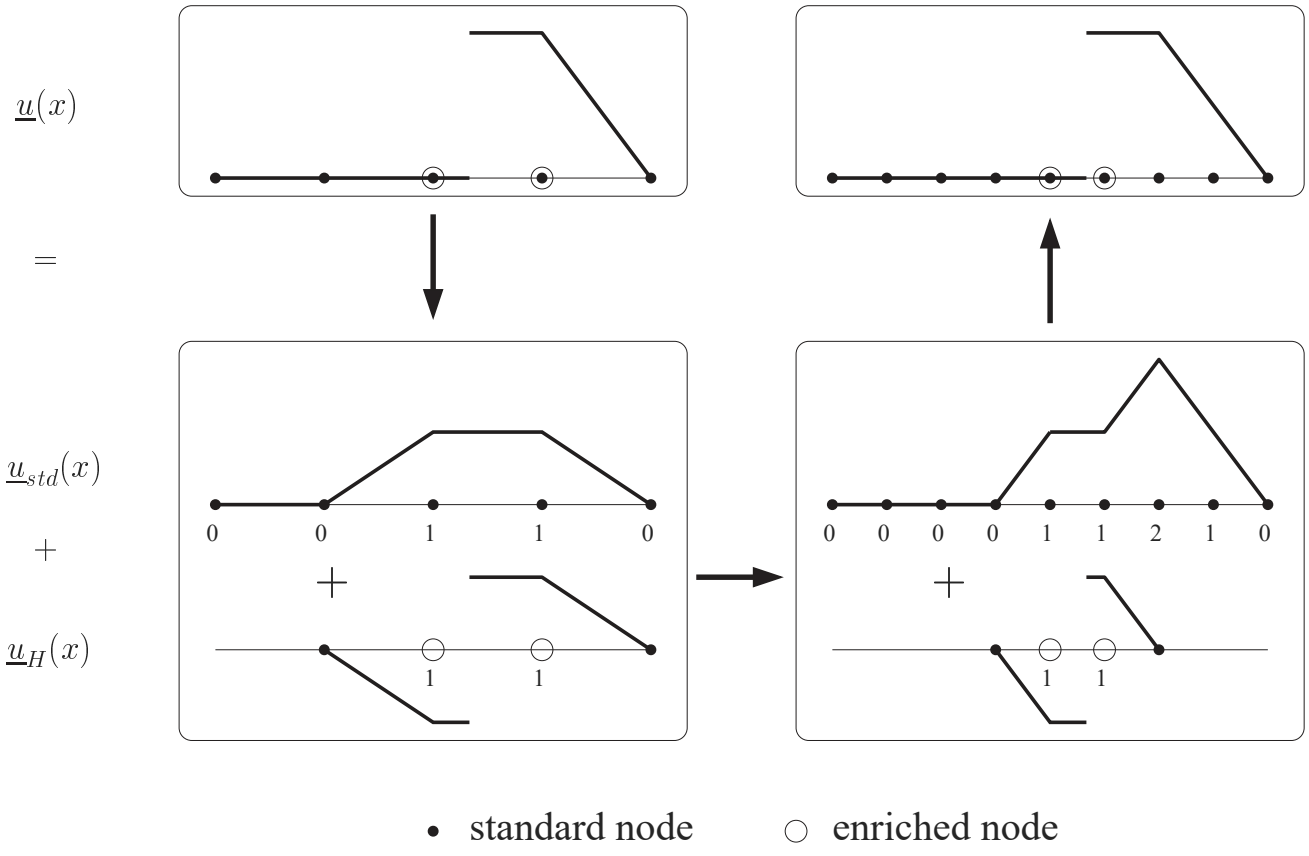

Figure 3. *Prolongation process with compatible enrichments. Only a cut enrichment is used here. The numbers below the nodes are the dof values*

Concerning the second set of nodes $\mathcal{S}_2$, the analysis is quite different. Indeed, they are enriched only with the H function, however the displacement field on the coarse mesh is enriched with H and γ_i functions (see for instance Figure 4b where the $\gamma_1(\underline{x}) \sum_{i \in \mathcal{N}_{sing}} (N_i(\underline{x}) b_{1i})$ function is not zeroed on $\underline{x}_b$,$\underline{x}_c$, $\underline{x}_h$, $\underline{x}_i$). In this respect, Equation [17] is no more verified, consequently these nodes are incompatible enriched ones. Degrees of freedom on the fine mesh are no more uniquely defined for identification. In this case, the adopted strategy consists in interpolate separately standard fields and enriched fields, even if they are not of the same type. As a consequence, the standard part of the displacement at $\underline{x}_b$, $\underline{x}_c$, $\underline{x}_h$, $\underline{x}_i$ is interpolated from the standard

part of the coarse displacement field and in a similar way for the enriched part. For instance, one obtains the following relations for node b:

$$\underline{u}_b = \sum_{i\in\{1,2,5,6\}} \underline{u}_i N_i(\underline{x}_b) \quad [31]$$

$$\underline{a}_b = \left(\sum_{i\in\{1,6\}} \underline{a}_i N_i(\underline{x}_b) H(\underline{x}_b) + \sum_{i\in\{2,5\}} \sum_{j=1}^{4} \underline{b}_j i N_i(\underline{x}_b) \gamma_j(\underline{x}_b) \right) \diagup H(\underline{x}_b) \quad [32]$$

In fact this configuration is rather easy to treat, since there is the only H enriched function on the fine mesh. Furthermore, this is the only possible case in practice (with a topological enrichment and a hierarchical elements strategy): indeed, an enriched node with γ_i functions necessarily brings to the element which contains the crack tip. And this node necessarily corresponds to the nodes of the coarse mesh linked to the element cut by the front (see Figure 2). Let notice that in the case of a geometrical enrichment strategy and hierarchical elements, one would meet the same particular cases (compatible and incompatible enrichments).

One has to see that this strategy (Equations [31] and [32]) introduces local numerical errors in the interpolation (see Section 4.1.1 and Figure 8e). This error is inevitable since the interpolation space of the displacement field is not the same between the coarse and the fine scales. However, it is important to notice that this error is local in space and of the order of the size of an element. In this respect, this corresponds to a high frequency error which will be smoothed with the first relaxation step of the multi-grid algorithm.

4. Examples

In this section, one considers a first example in the aim to illustrate the good numerical properties of the multi-scale operators previously defined in the context of the extended finite element method. The second example is a very simplistic application of the method to mixed mode crack growth simulation: indeed, in this case multi-grid strategy is not essential, however this illustrates the possibility of the method in the case of real applications where one have a very complex initial mesh which can not be changed. In this respect, a multi-grid strategy coupled with X-FEM can be very useful in the aim to locally define the good spatial scales which allow to simulate mixed mode fatigue crack growth with no re-meshing techniques.

The different parameters of the method and their influence on the convergence and the accuracy are studied. On the coarsest scale a direct solver is used and a Jacobi preconditioned conjugate gradient solver is used for relaxation steps.

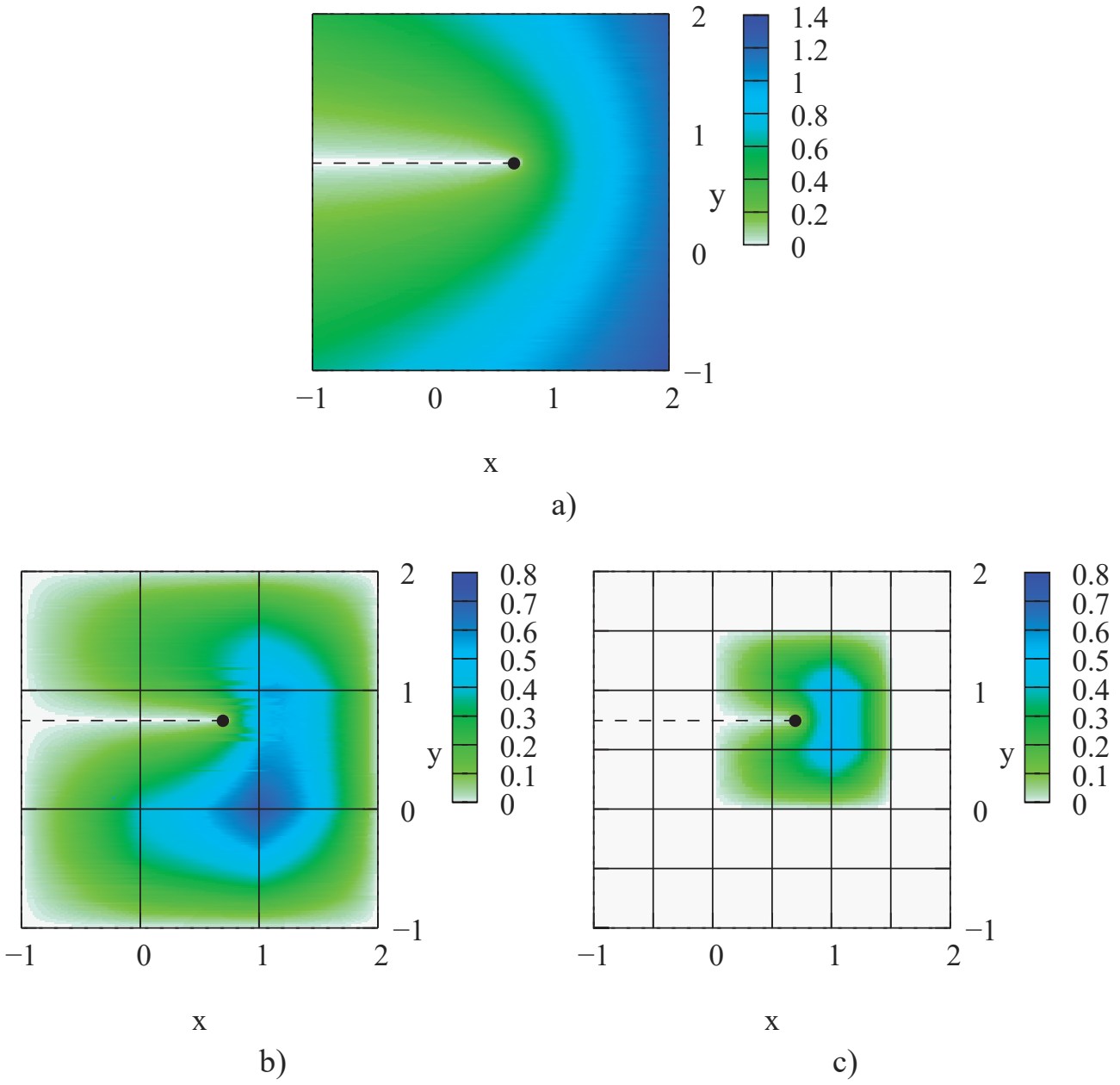

Figure 4. *Function* $\gamma_1(r,\theta) = \sqrt{r}\cos(\theta/2)$. γ_1 *is independent on the discretization and depends only on the crack geometry represented with a dashed line (a) . The local nature of the enrichments is due to the term* $\gamma_1(\underline{x}) \sum_{i \in \mathcal{N}_{sing}} (N_i(\underline{x}) b_{1i})$ *as illustrated on (b) and (c) for the two meshes of Figure 2. All the* b_{1i} *are set to* 1

4.1. *Case of a tensile plate with a horizontal crack*

One considers a plate subjected to a tensile stress ($\sigma_{yy} = 10\ MPa$) with a horizontal crack (see Figure 4 for the geometry). One considers a linear elastic homogeneous isotropic behaviour with the following Young's modulus and Poisson's ratio: $E = 200\ GPa$, $\nu = 0.33$. The crack tip is defined by the coordinates (x_f, y_f). In this case, one chooses the following values: $x_f = 3.45\ cm$ and $y_f = 3.5522\ cm$. The crack does not follow the boundary of the finite elements and is essentially solicited in mode I. The considered meshes are structured hierarchical linear quadrangle finite

element meshes (see Figure 6). The solution computed with the mesh 3 is plotted on Figure 7.

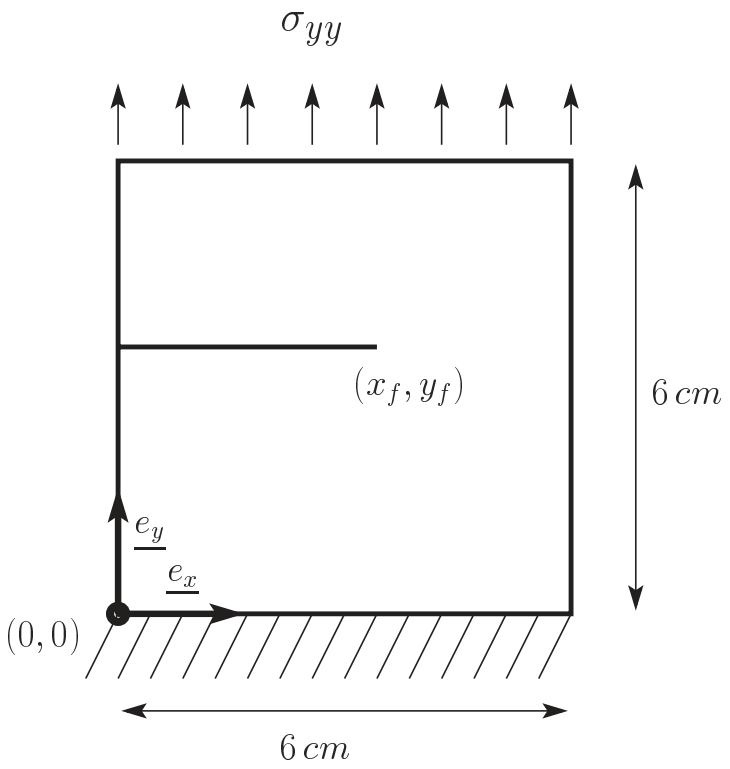

Figure 5. *Geometry of the plate*

4.1.1. *Influence of relaxation steps and multi-scale operators*

In this study, one wants to illustrate the contribution of each grid and the iterations on the solution with the X-FEM multi-grid strategy. In this respect, the error $\underline{e}$ is

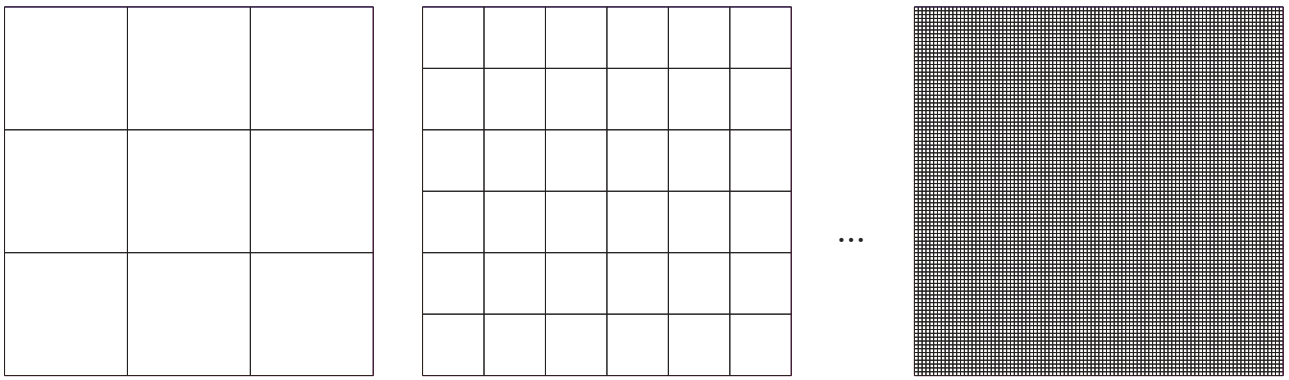

Figure 6. *Some of the meshes used in the multi-grid strategy*

defined as the difference between the exact numerical solution $\underline{u}$ (which is known in this case) and the current numerical solution $\underline{\tilde{u}}$:

$$\underline{e} = \underline{u} - \underline{\tilde{u}} \qquad [33]$$

Indeed, this quantity is a good error indicator on the quality of the numerical solution obtained at each step of the X-FEM multi-grid algorithm.

Figure 8 shows the error field at each step of a two meshes multi-grid cycle. The fine mesh is the mesh 3 with 1288 elements. All the views are plotted with the same amplification factor. The algorithm is initialized with a null vector, so the initial error is equal to the exact numerical solution $\underline{u}$ (Figure 8a).

The effect of the first relaxations ν_1 is not significant: the Euclidian norm of the error decreases from $3,2.10^{-3}\ m$ to $2,9.10^{-3}\ m$. The displacement field is here close to a rigid body move on the upper part of the structure. As a consequence, it is clear that the first corrections are essentially linked to a low frequency error, that is to say linked to the coarse mesh. In this respect, the next correction on the coarse grid is clearly efficient and contributes to decrease the low frequency error of the solution since the Euclidian norm of the error equals $8,9.10^{-5}\ m$. In the same way, for the moment, the second relaxation step does not decrease significantly the error (error= $8,8.10^{-5}\ m$). However, one can notice on Figure 8e that the correction on the coarse mesh has introduced a high frequency error. This error is present on all the domain but is more important near the crack tip because of the incompatible enrichments. Furthermore, on Figure 8f, it is also clear that relaxation steps quickly eliminates these high frequency errors and in particular the second relaxation step.

4.1.2. *Influence of the multi-grid parameters*

The two relaxation parameters ν_1 and ν_2 plus the number of cycles γ can have a great influence on the convergence of the X-FEM multi-grid algorithm. The interesting quantities to compare are the CPU time with the multi-grid cycles at convergence N_c. Tables 1, 2 and 3 present the results for different sizes of the problem. The number of cycles at convergence is a non integer number. Indeed, it is obtained by interpolation between the two last cycles since the convergence can be achieved before the last relaxation step. The accuracy is chosen equal to $\varepsilon = 10^{-8}$ (cf. [10]). The CPU time concerns the relaxation steps t_{relax}, but not the prolongation and restriction steps t_{PR}. However, t_{PR} can be non negligible when $\nu_1 + \nu_2$ is small.

One can notice that single V-cycles ($\gamma = 1$) are not very efficient. The number of operations per cycle with $\gamma = 1$ is lower than with $\gamma = 2$ or 3, however this not compensates the high number of necessary cycles. With $\gamma = 2$, the number of cycles greatly decreases of the order of 4 or 5 (Table 3). The CPU time also decreases. Furthermore, the total iteration number $\nu_1 + \nu_2$ is also important. In this particular case, a small number of relaxation steps is sufficient to converge ($\nu_1 + \nu_2 = 3$). Decreasing ν_1 and ν_2 involves a small increasing of N_c however this is highly compensated by the decreasing of the total number of iterations. From $\nu_1 + \nu_2 = 8$ to $\nu_1 + \nu_2 = 3$, one observes on Table 3 an increasing for N_c of 1.3, but a decreasing for the CPU

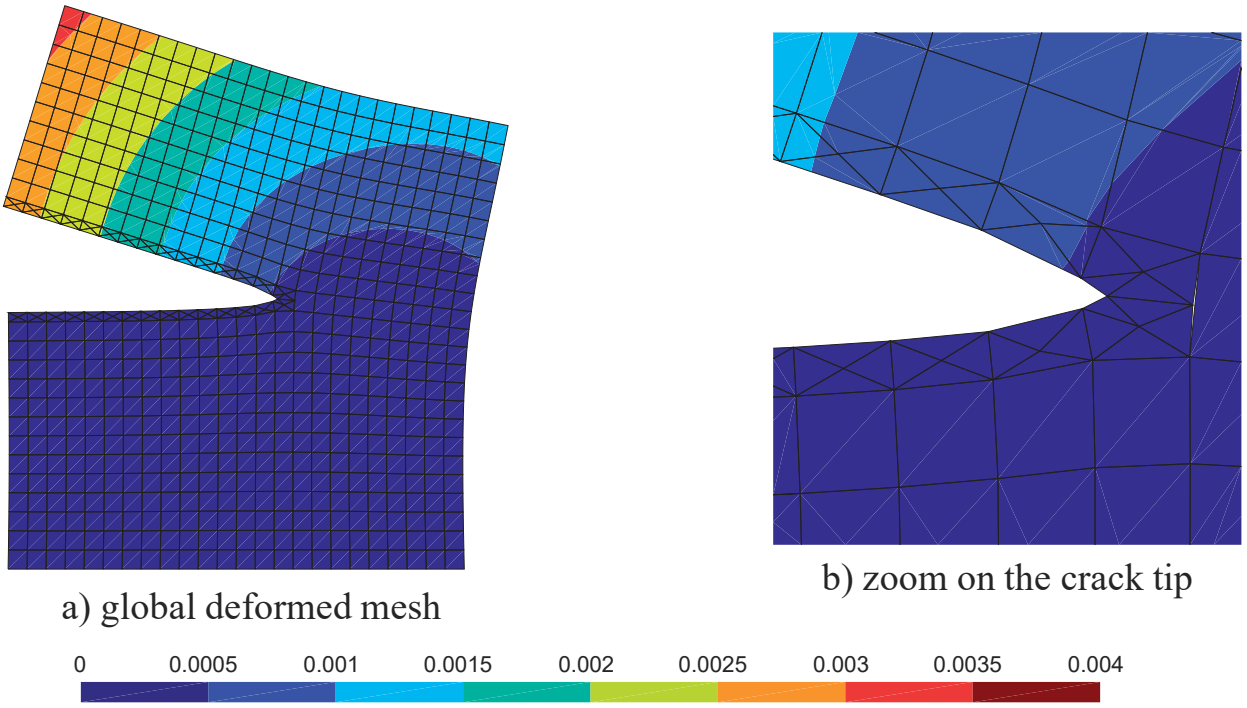

Figure 7. *Displacement field and colormap of its euclidian norm (in m) of the cracked tensile plate (a) and zoom on the crack tip (b)*

time of 1.7. With the choice $\gamma = 3$, the number of multi-grid cycles still decreases, however the gain does not compensate the high number of iterations per cycle. As a consequence, it seems that $\gamma = 2$ is an optimal parameter for this example. Furthermore, considering the results for the three different meshes, one observes that with ν_1, ν_2 and γ fixed, the number of multi-grid cycles N_c is almost constant. This remark is very similar to the one obtained by Parsons et Hall in (Parsons *et al.,* 1990a). They also propose to evaluate the total number of operations per cycle N_oc with the following relation:

$$N_{oc} = C_V \left(1 + \frac{\gamma}{4} + \left(\frac{\gamma}{4}\right)^2 + \ldots + \left(\frac{\gamma}{4}\right)^{M-2}\right) n + N_{ds} \qquad [34]$$

where n is the problem size, N_{ds} is the number of operations needed for the exact resolution with the initial coarsest mesh and M the number of grids. If M is sufficiently great, then the resolution on the coarsest mesh has a very small numerical cost (compared to the finest mesh cost) and one can neglect N_{ds}. C_V is a proportional coefficient between n and $N_{oc} - N_{ds}$ in the case of a two scale resolution. C_V depends essentially on ν_1 and ν_2. If one assumes that the arithmetic suit [34] is stabilized, one can consider that N_{oc} is proportional to n (N_{oc} is in $O(n)$). Indeed, from the assumption that the number of multi-grid cycles N_c is constant (N_c is in $O(1)$), one deducts that the total number of operations needed to converge N_{tot} is in $O(n)$ since $O(1).O(n) = O(n)$. Figure 9 represents the evolution of the CPU time t_{relax} with respect to the size of the problem for different values of ν_1 and ν_2 with $\gamma = 2$. One also represent the linear interpolated curves for the X-FEM multi-grid and a preconditioned

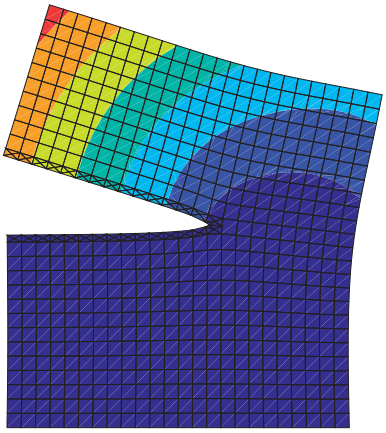

max error : $3,2.10^{-3}m$
a) initial error (equal to the solution)

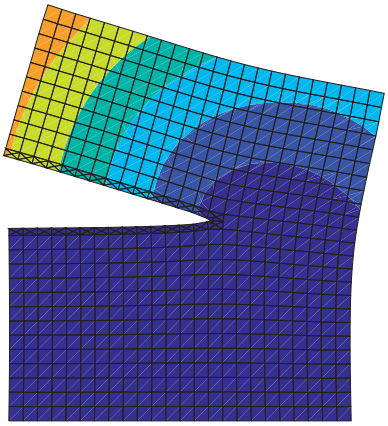

max error : $2,9.10^{-3}m$
b) error after $\nu_1 = 5$ iterations

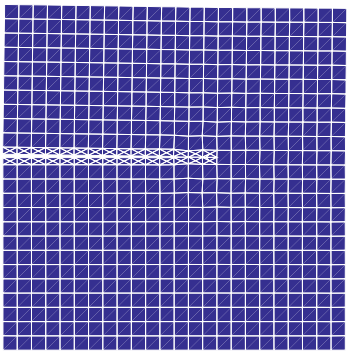

max error : $8,9.10^{-5}m$
c) error after correction on the coarse mesh

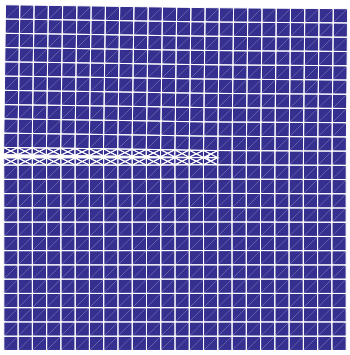

max error : $8,8.10^{-5}m$
d) error at the end of the cycle after $\nu_2 = 1$ iteration

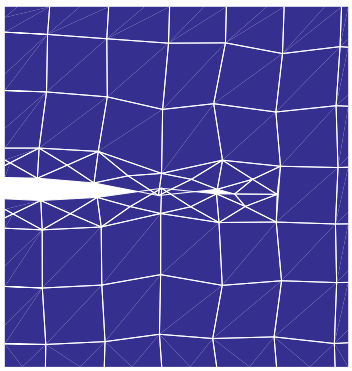

e) zoom on the error after the correction step on the coarse mesh

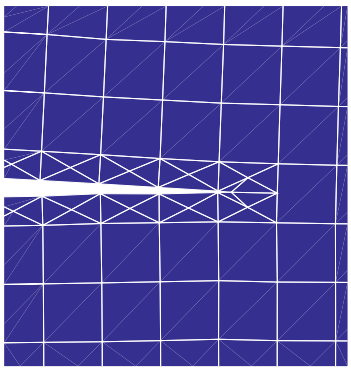

f) zoom on the error at the end of the cycle after $\nu_2 = 1$ iteration

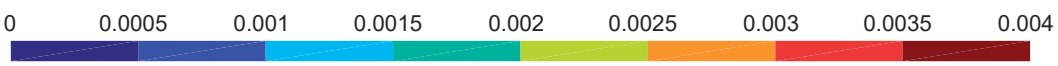

Figure 8. *Normalized error scalar field (in m) plotted on the amplified error vector field at differents steps of the multi-grid algorithm. All the figures are plotted with the same amplification factor. A zero-error field would be represented on an underformed shape*

conjugate gradient (in $O(n^{3/2})$). These results confirm the previous assumption, that is to say a convergence of the X-FEM multi-grid algorithm in $O(n)$.

Table 1. *CPU time and number of multi-grid cycle to convergence for mesh 3 (1288 dofs). The conjugate gradient method reach convergence at* $0.05\ s$

ν_1 and ν_2	γ	cpu time in s	N_c
$\nu_1 = 3\,,\nu_2 = 2$	1	0.21	27.5
$\nu_1 = 5\,,\nu_2 = 3$	2	0.11	5.3
$\nu_1 = 3\,,\nu_2 = 2$	2	0.10	6.5
$\nu_1 = 2\,,\nu_2 = 1$	2	0.11	8.8
$\nu_1 = 3\,,\nu_2 = 2$	3	0.27	7.9
$\nu_1 = 2\,,\nu_2 = 1$	3	0.30	7.6

Table 2. *CPU time and number of multi-grid cycle to convergence for mesh 4 (4848 dofs). The conjugate gradient method reach convergence at* $0.25\ s$

ν_1 and ν_2	γ	cpu time in s	N_c
$\nu_1 = 5\,,\nu_2 = 5$	1	0.64	20.0
$\nu_1 = 3\,,\nu_2 = 2$	1	0.63	33.5
$\nu_1 = 5\,,\nu_2 = 3$	2	0.25	5.7
$\nu_1 = 3\,,\nu_2 = 2$	2	0.23	6.9
$\nu_1 = 2\,,\nu_2 = 1$	2	0.20	7.5
$\nu_1 = 3\,,\nu_2 = 2$	3	0.49	7.0
$\nu_1 = 2\,,\nu_2 = 1$	3	0.36	6.9

Table 3. *CPU time and number of multi-grid cycle to convergence for mesh 5 (18880 dofs). The conjugate gradient method reach convergence at* $2.40\ s$

ν_1 and ν_2	γ	cpu time in s	N_c
$\nu_1 = 5\,,\nu_2 = 5$	1	4.12	28.5
$\nu_1 = 5\,,\nu_2 = 3$	2	1.04	5.8
$\nu_1 = 3\,,\nu_2 = 2$	2	0.90	6.9
$\nu_1 = 2\,,\nu_2 = 1$	2	0.61	7.6
$\nu_1 = 5\,,\nu_2 = 3$	3	1.46	4.1

4.2. *Example of a mixed mode crack growth simulation*

In this example, one applies the X-FEM multi-grid strategy in the case of a mixed mode crack growth simulation (see Figure 10 for the geometry and the loading). Furthermore, one assumes a linear elastic homogeneous isotropic behaviour. In this respect, the Young's modulus equals 200 GPa and the Poisson's ratio is 0.3.

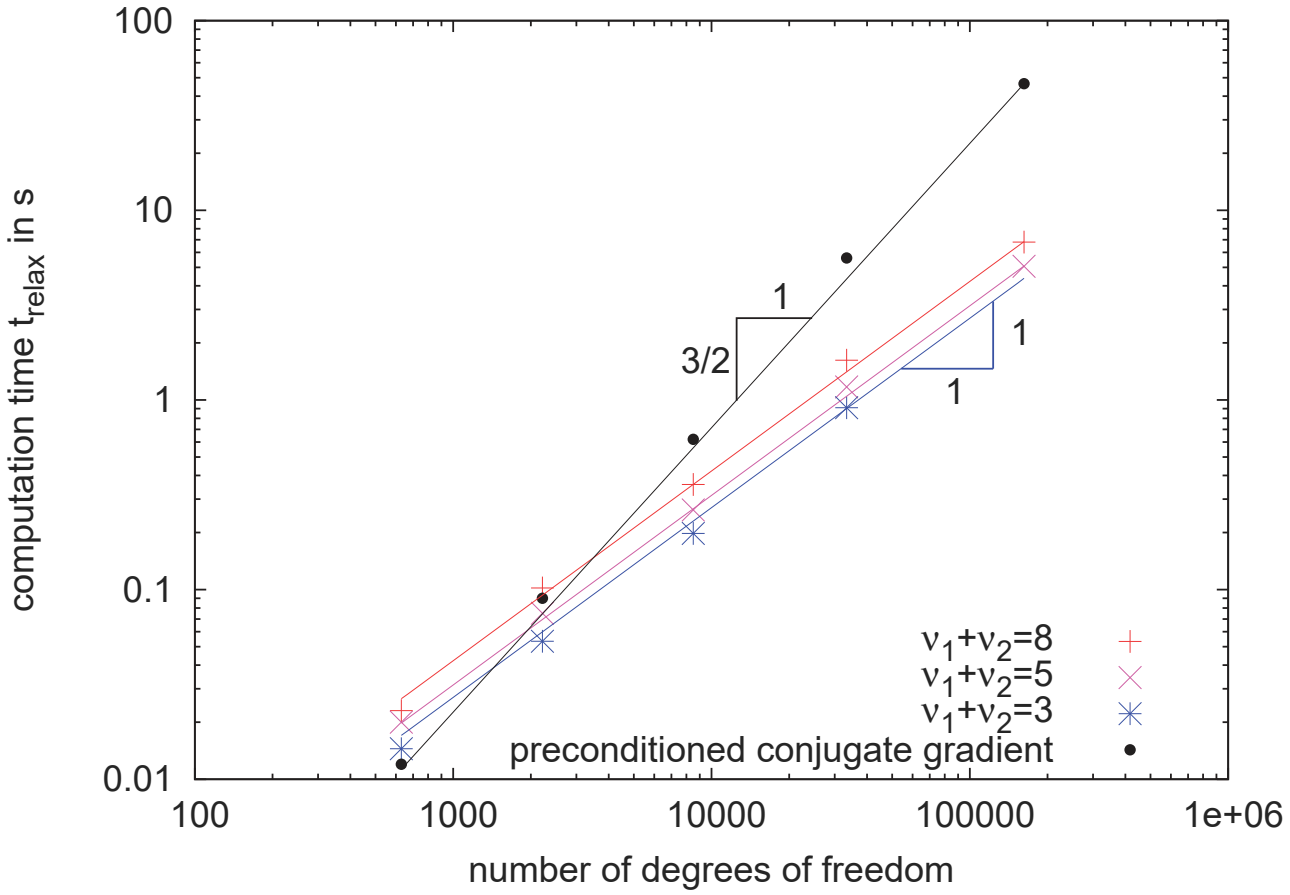

Figure 9. *Computation time and fit for preconditioned conjugate gradient and multi-grid method with different values of* $\nu_1 + \nu_2$ *and* $\gamma = 2$

The different grids are represented on Figure 11. The crack and the hole are represented with respectively generalized Heaviside and Heaviside enrichment functions. The mesh 0 is very coarse, and meshes 1 and 2 are obtained from mesh 0 by subdividing elements in a predefined zone in the aim to accurately describe the path of the crack and the stress gradients during its propagation and the influence of the hole on it. However, it is clear in this example that the different grids are not fine enough to accurately solve the mechanical problem (influence of the stress concentration factor). This is not the aim of this simulation: one only wants to qualitatively validate the X-FEM multi-grid algorithm, and in particular notice that, even if the initial crack is very small on the coarse mesh (see Figure 11), the crack is well "captured" by the solver because of its good representation on the fine mesh. Indeed, the most important thing is to define the fine mesh accordingly with the spatial space scales you want to "capture". One has to notice that the same geometrical support was used on each level to describe the crack geometry. A complex crack geometry would require a lot of work to get an accurate quadrature on the corsest levels. However, a such accurate computation is useless since the only level of interest is the finest one. Indeed, one recalls that the coarse level has no mechanical meaning and is only usefull to increase

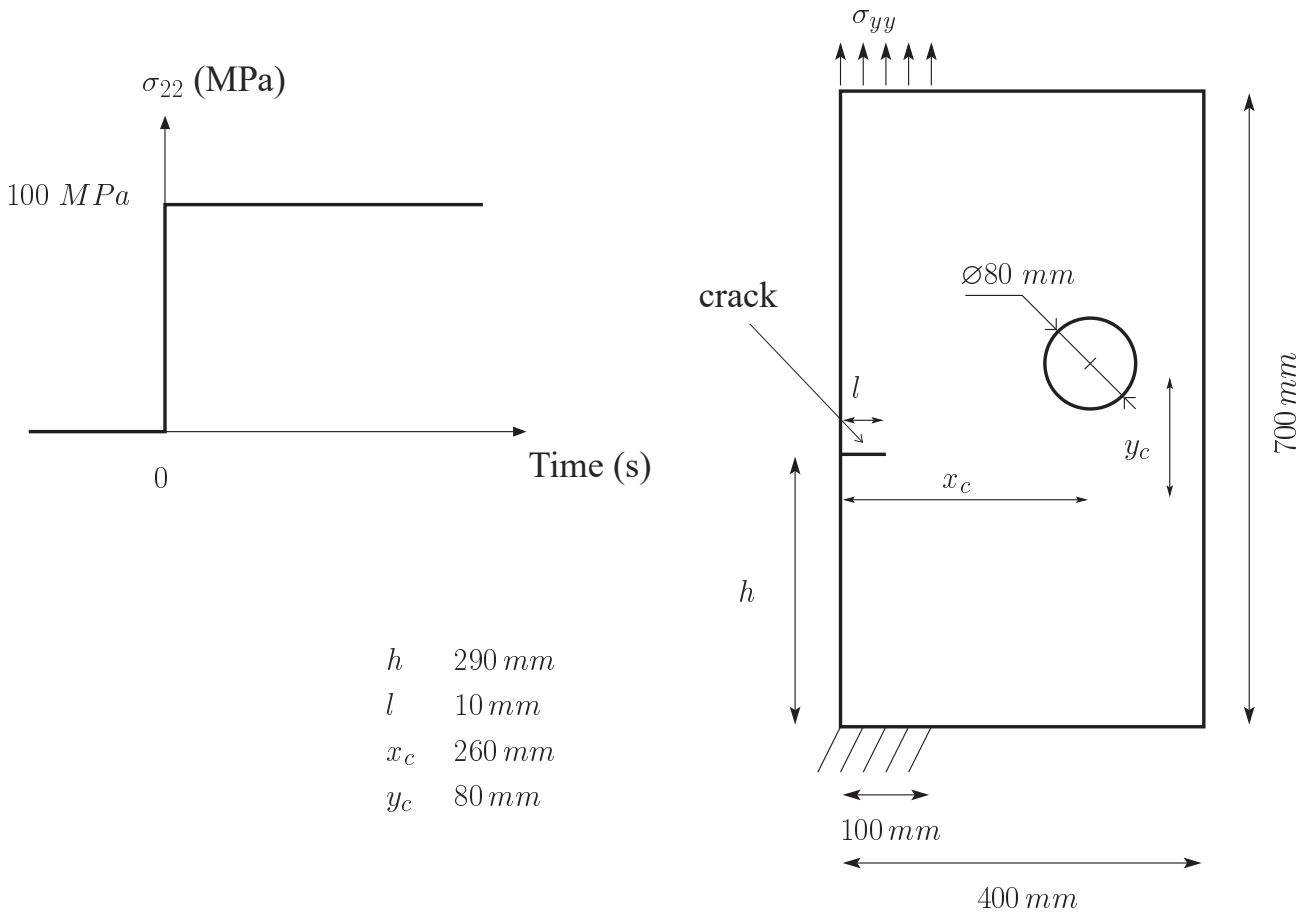

Figure 10. *Description of geometry, loading and boundary conditions of the second example*

the convergence rate of the fine problem. In this respect, a coarsest representation of the coarse mesh should be sufficient.

Stress intensity factors are calculated with the interaction integral which can be written as follow (Gosz *et al.,* 1998) :

$$M^{(1,2)} = \int_{\Gamma} \left[\sigma_{ij}^{(1)} \varepsilon_{ij}^{(2)} \delta_{1j} - \sigma_{ij}^{(1)} \frac{\partial u_i^2}{\partial x_1} - \sigma_{ij}^{(2)} \frac{\partial u_i^1}{\partial x_1} \right] n_j d\Gamma \qquad [35]$$

where $\underline{n}$ is the unit normal vector of the contour Γ. Superscripts ^{1} and ^{2} are related respectively to the actual and to an auxilliary state. In the case of plane strain assumption, stress intensity factors K_I and K_{II} can be obtained by the use of the auxiliary fields respectively in mode I and II :

$$K_I^{(1)} = E/2(1-\nu^2) M^{(1,ModeI)} \qquad [36]$$

$$K_{II}^{(1)} = E/2(1-\nu^2) M^{(1,ModeII)} \qquad [37]$$

The presented results on Figure 12 correspond to stress intensity factors I and II and the energy release rate G depending on the crack length. Furthermore, the deformed mesh with the Euclidian norm of the displacement field is plotted on Figure 14.

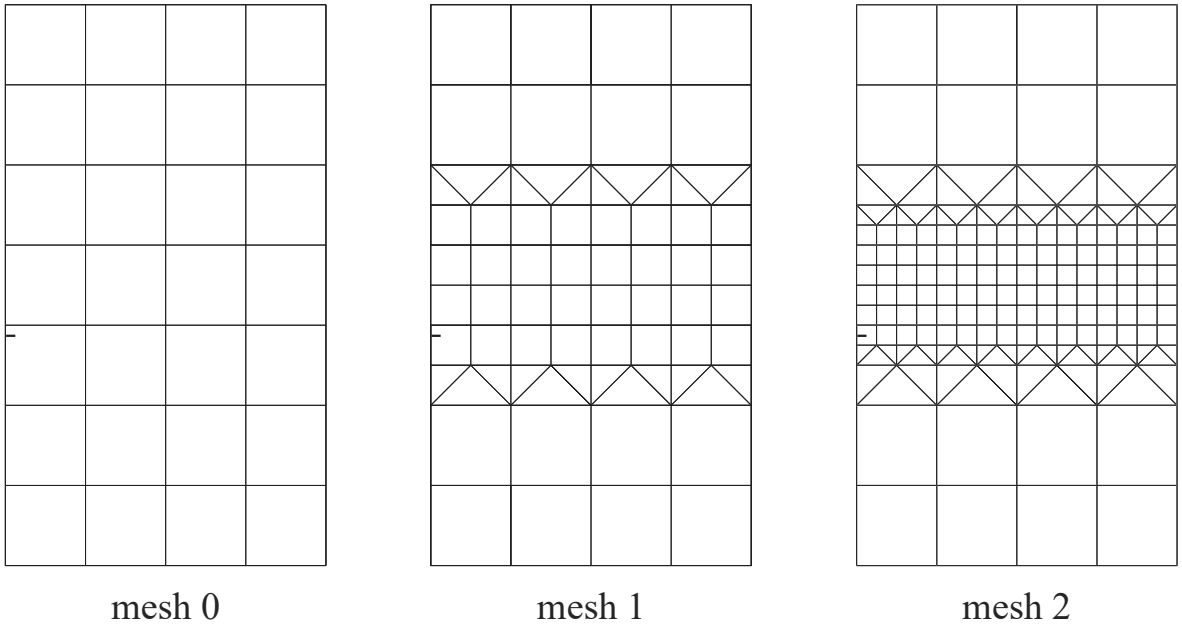

Figure 11. *The different meshes used. The initial crack is also represented*

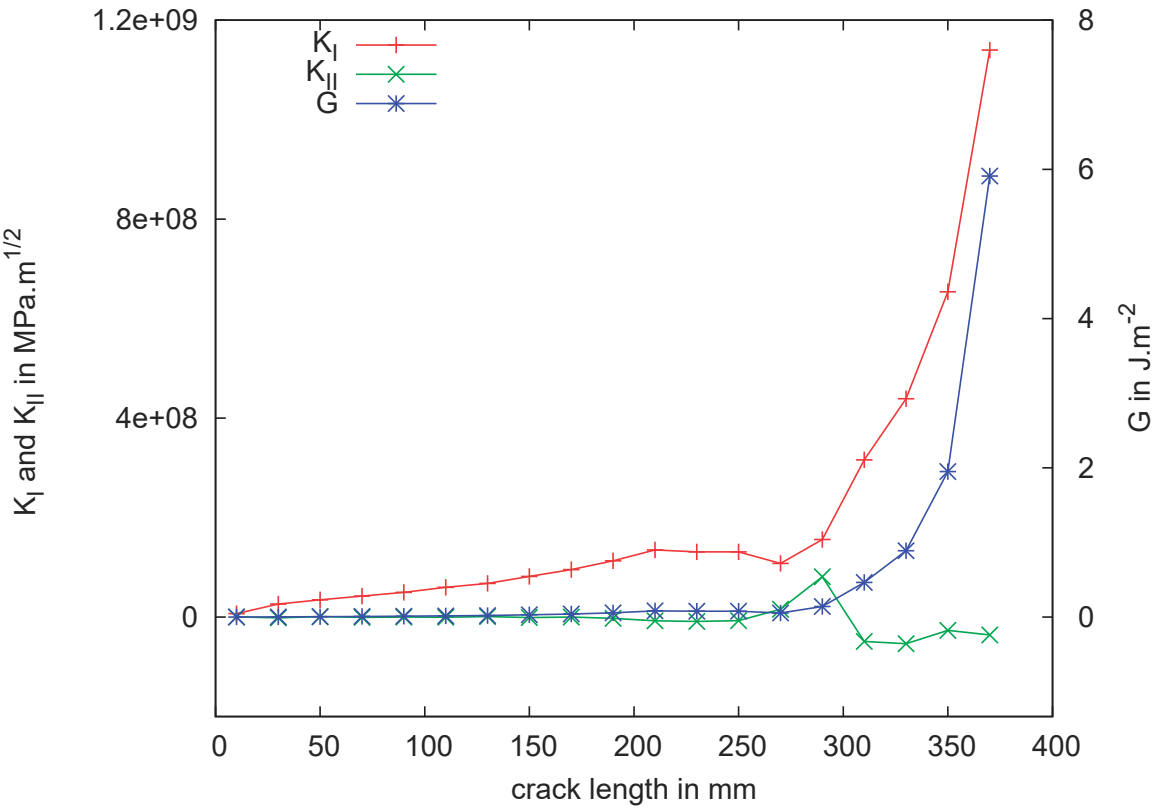

Figure 12. *Stress intensity factors K_I, K_{II} and energy release rate G*

Figure 13 represents the convergence results of the X-FEM multi-grid algorithm (with $\gamma = 2$, $\nu_1 = 5$ and $\nu_2 = 3$) for different positions of the crack tip during the propagation. One observes a small influence of the crack tip position on the convergence rate, in particular close to the hole. However, in a general point of view, a good con-

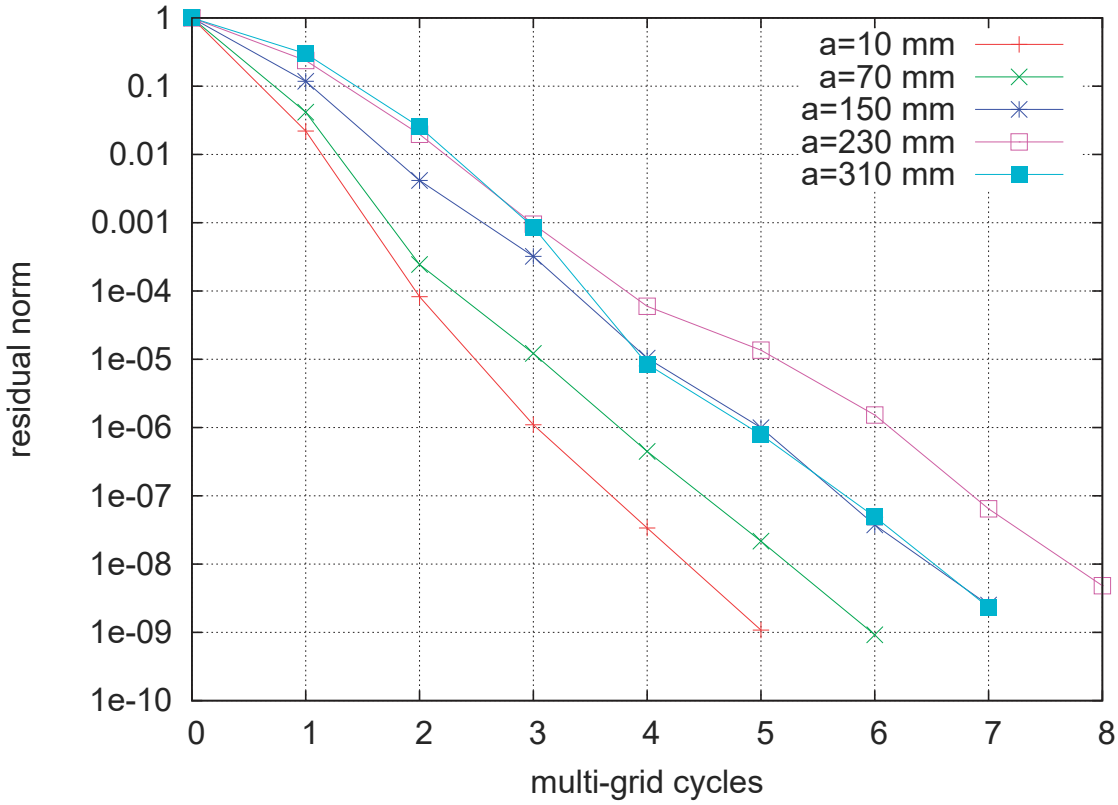

Figure 13. *Convergence of the multi-grid algorithm for different crack length a*

vergence rate is obtained since for each multi-grid cycle the residual norm decreases by one decade.

5. Concluding remarks

A multi-grid extended finite element method was presented. In this respect, specific multi-scale operators where developed. Even the prolongation and restriction steps can generate local errors, it is shown that these ones are smoothed very efficiently by the relaxation steps. Furthermore, the well-known convergence rate of the classical multi-grid finite element method is preserved: indeed, coupling X-FEM and the multi-grid strategy involves a similar convergence rate. In a general point of view, this approach can be very useful to automatically take into account various adapted spatial space scales (for cracks, holes, inclusions, refined regions...) which are not necessarily described in the initial fixed mesh (coming from engineering applications). An application of the X-FEM multi-grid strategy was proposed for elastic mixed mode crack growth simulations. However, further studies are needed to the extension of the method to nonlinear behaviours and tri-dimensional crack growth simulations.

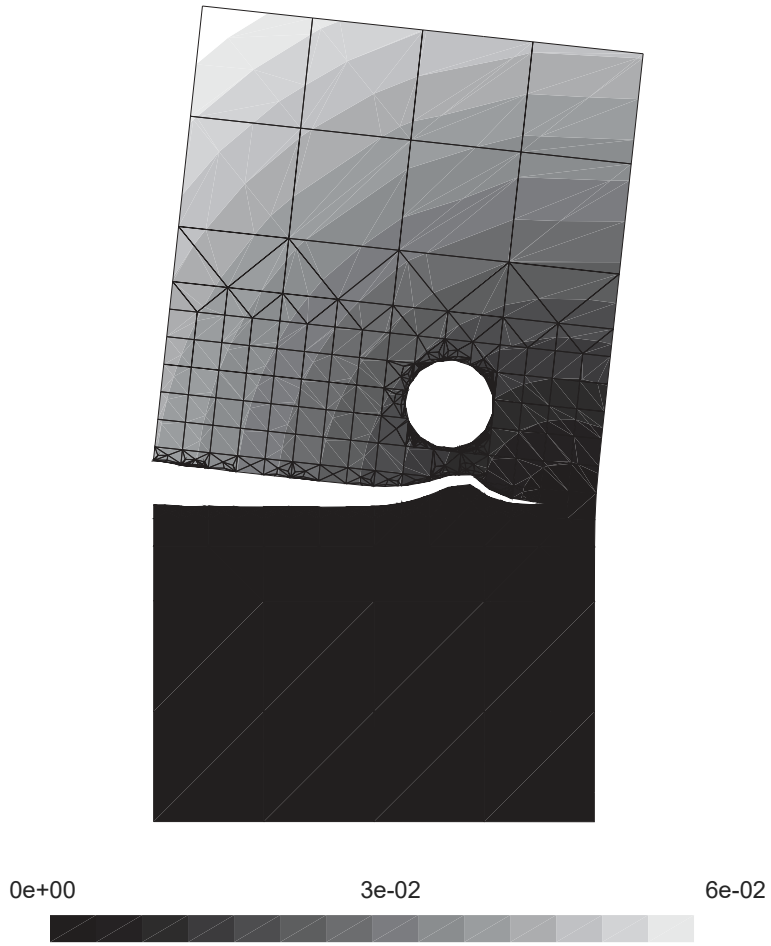

Figure 14. *Displacement field and colormap of its euclidian norm (in m) for $a = 370\ mm$*

6. References

Béchet E., Minnebo H., Moës N., Burgardt B., « Improved implementation and robustness study of the X-FEM for stress analysis around cracks », *International Journal for Numerical Methods in Engineering*, vol. 64, n° 8, p. 1033-1056, june, 2005.

Brandt A., « Multi-level adaptative technique (mlat) for fast numerical solution to boundary value problems », *Lecture Notes in Physics*, 1977.

Dureisseix D., Une approche multi-échelle pour des calculs de structures sur ordinateurs à architecture parallèles, PhD thesis, LMT Cachan, n.d.

Elguedj T., Gravouil A., Combescure A., « A mixed Augmented Lagrangian eXtended Finite Element Method for modelling elastic-plastic fatigue crack growth with frictional contact », *International Journal for Numerical Methods in Engineering, submitted*, 2005.

Feyel F., « A multilevel finite element method (FE2) to describe the response of highly non-linear structures using generalized continua », *Computer Methods in Applied Mechanics and Engineering*, vol. 192, n° 28-30, p. 3233-3244, july, 2003.

Fish J., Yuan Z., « Multiscale enrichment based on partition of unity », *International Journal for Numerical Methods in Engineering*, vol. 70, p. 1341 - 1359, 2004.

Gosz M., Dolbow J., Moran B., « Domain integral formulation for stress intensity factor computation along curved three-dimensional interface cracks », *International Journal of Solids and Structures*, 1998.

Gravouil A., Combescure A., « Multi-time-step and two-scale domain decomposition method for non-linear structural dynamics », *International Journal for Numerical Methods in Engineering*, 2003.

Guidault P., Allix O., Champaney L., Navarro J., « A multiscale computational strategy for crack propagation with local enrichment », *USNCCM 8 - 8th US National Congress on Computational Mechanics*, 2005.

Lubrecht A. A., Venner C. H., *Multilevel methods in lubrication*, Elsevier, 2000.

Melenck J. M., Babuška I., « The partition of unity finite element method: Basic theory and applications », *Computer Methods in Applied Mechanics and Engineering*, vol. 139, p. 289-314, 1996.

Moës N., Dolbow J., Belytchko T., « A finite element method for crack growth without remeshing », *International Journal for Numerical Methods in Engineering*, vol. 46, p. 131 - 150, 1999.

Parsons I. D., Hall J. F., « The multigrid method in solid mechanics : Part I – algorithm description and behaviour », *International Journal for Numerical Methods in Engineering*, 1990a.

Parsons I. D., Hall J. F., « The multigrid method in solid mechanics : Part II – practical applications », *International Journal for Numerical Methods in Engineering*, 1990b.

Ribeaucourt R., Baïetto-Dubourg M., Gravouil A., « A mixed fatigue crack growth model applied to rolling contact fatigue », *3rd World Tribology Congress, Washington, D.C., USA*, september 12-16, 2005.

Stazi F., Finite element method for cracked and microcracked bodies, PhD thesis, Università di Roma "La Sapienza", april, 2003.